Science

AAAS

Supplementary Materials for

Vortex beams of atoms and mole

Alon Luski *et al.*

Corresponding author: Edvardas Narevicius, edn@weizmann.ac.il

The PDF file includes:

Materials and Methods
Supplementary Text
Figs. S1 to S6
Table S1

Materials and Methods

<u>Detection</u>

The metastable states of helium and neon have an excess energy of about 20 eV and 16 eV respectively. Virtually any interaction of these atoms with a surface causes relaxation and decay to the ground state. As a result, these metastable states enabled efficient time and position-sensitive diffraction image measurement using a micro-channel plate detector. The MCP was assembled with a phosphor screen, and the light emitted from each impact event was recorded through a viewport by a camera outside the vacuum chamber. The image on the camera screen was processed in real time to localize each particle's using a centroiding algorithm. This algorithm calculated the center of mass of each event (the impact spots are several pixels wide) and return a position in a sub-pixel value that matches the resolution of a single channel of the MCP, about 15 μm. The recorded positions are then presented in 2D histogram with a chosen bin size.

<u>Grating fabrication</u>

We used silicon nitride membranes, 20 nm thick, on transmission electron microscope grids purchased from TEMwindows. To obtain good adhesion of the electron-beam sensitive resist to the membranes, we applied delicate oxygen and argon plasma in a plasma ashing system, using 150 W of plasma power for 5 minutes, and flow rates of 3 standard cubic centimeters per minute (sccm) for oxygen and 1 sccm for argon at a pressure of 150 mTorr. We spin-coated the membranes with a ZEP-520A resist diluted in anisole (1:1) at a speed of 4000 rpm, resulting in a 100 nm thick resist.

We exposed the pattern by electron beam lithography using a RAITH eLINE Plus system. We used a 30 keV accelerating voltage and a 10 microns aperture, yielding a beam current of 25pA. In the exposure step, we applied a dose of 150 $\mu C/cm^2$. The sample was then developed in n-Amyl acetate for 1 minute and rinsed in isopropyl alcohol for half a minute.

To etch the silicon nitride film, we applied a dry etching technique using the inductively coupled plasma mode in the SPTS Technologies Ltd Rapier system. We applied 50 sccm of CHF_3 and 10 sccm of Argon plasma with a coil power of 75 W, a bias power of 50 W and a pressure of 20 mTorr for 35 seconds. Finally, we added a short oxygen plasma process using the Direct Sample Insertion mode at 100 sccm and a pressure of 35mTorr for 25 seconds, to remove the residual ZEP resist.

Supplementary Text

Grating and array effects

The experimental setup contained several differences from the ideal theoretical diffraction model used for designing the gratings. For example, the gratings were fabricated in a periodic array to increase the count rate. The particle source is also not an ideal, monochromatic plane wave. Here we provide an analysis of the effects due to these and other differences between the experiment and the ideal model.

In Fig. S1b, we first show a calculation of diffraction from a single forked grating. The dislocation leads to a phase singularity in the center of each order in the far field, which creates vortex ring images. When the entire mask structure with multiple grating units is taken into account, along with the atomic beam parameters, different blurring effects can be seen (Fig. S1d). Some of these are due to coherent effects: when the coherence length of a particle is not negligible in comparison with the spacing between grating units, paths of the same wave through different units will interfere. For example, a wave covering two neighboring grating units will produce a periodic grid-like structure with an angular spacing of $\theta_\omega = \lambda/\omega$, where ω is the center-to-center distance in the array (Fig S2).

Three additional blurring effects are due to incoherent aberrations. First, chromatic aberrations arise from the velocity spread of the supersonic beam, creating a compilation of images with slightly different scaling. In our experiment, with a valve cooled to 115 K of helium at 20 bar, we measured a 3% velocity spread (full width at half maximum) based on the spread of the time of flight of the detected particles through the setup, which leads to negligible blurring. The second effect is caused by non-point source illumination: due to the finite size of the skimmer apertures, particles from slightly different angles are able to pass through the grating. As a result, each grating creates a slightly blurred image compiled from diffraction into a distribution of angles. Finally, the pattern repetition creates a smearing of the image due to >2000 grating units present in the 50x50 μm array. All of these effects were taken into account in the simulation constructed for this work, and applied in the comparison presented in Fig. 4.

The slits of the forked gratings were etched into circular areas in the mask. These circular shapes were responsible for some of the structures observed around the beam diffraction orders. The effect is similar to the appearance of Airy disks in diffraction from a circular aperture. However, unlike gratings with edge-dislocations, circular apertures will not produce the phase singularities corresponding to the holes in the intensity images of vortex beams. This can be seen in Fig. S3, which presents a calculated diffraction image by a circular aperture containing a regular slit grating. The image contains a series of spots along with higher-order surrounding structures, lacking any phase singularities, with the highest intensity always located at the center of each diffraction order peak.
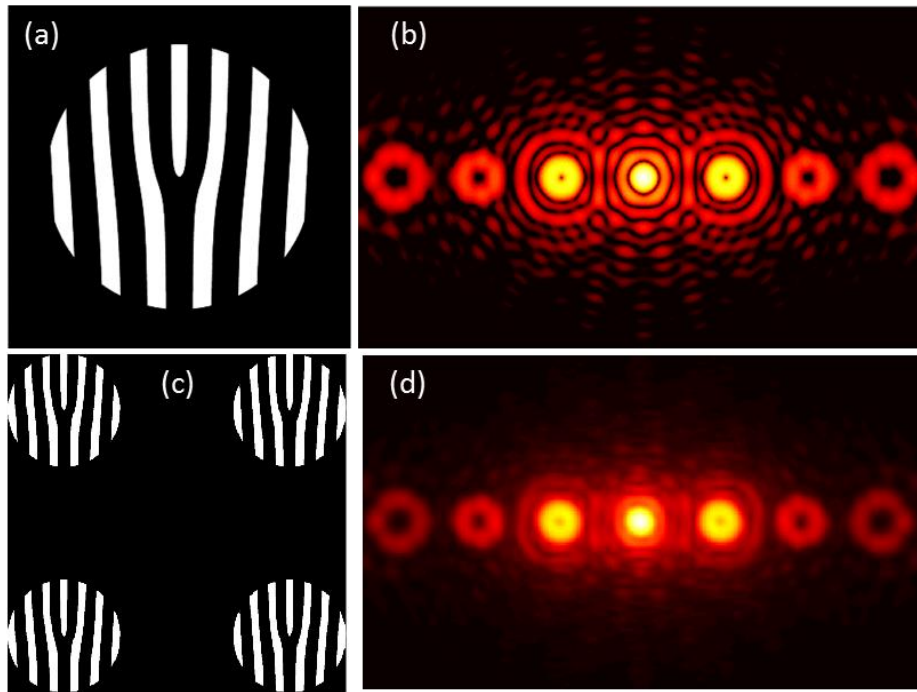
Figure S1: (a) Binary grating with a single-edge dislocation and calculated diffraction image (b). (c) Gratings in a unit cell repeat every 1.2 microns and diffraction image (d), calculated for a coherence length of 840 nm. The images were calculated for a grating with an open to blocked slit ratio of 4/6 and a periodicity of 100 nm. The intensity maps are in logarithmic scale.
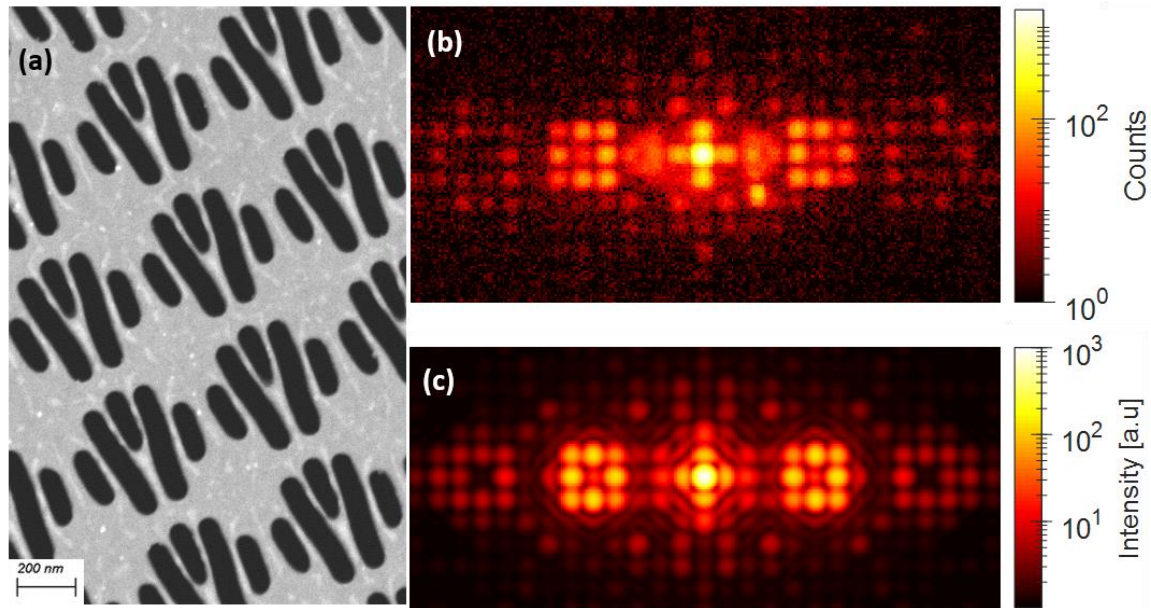
Figure S2: Coherent cross-talk between grating units. A beam with a coherence length of 840 nm was diffracted off an array of 450 nm diameter forked grating units with a 500 nm period (a), producing an image with additional small-scale diffraction patterns caused by the periodicity (b). The simulated image (c) reproduces these features. Note the absence of the dimer spots on either side of the zero-order spot in the simulated image.
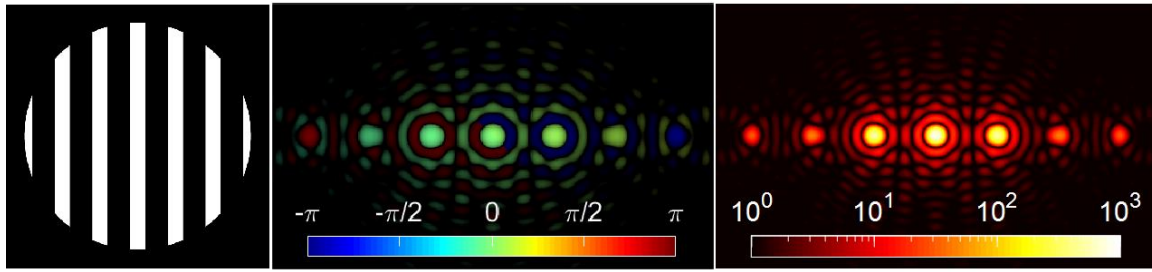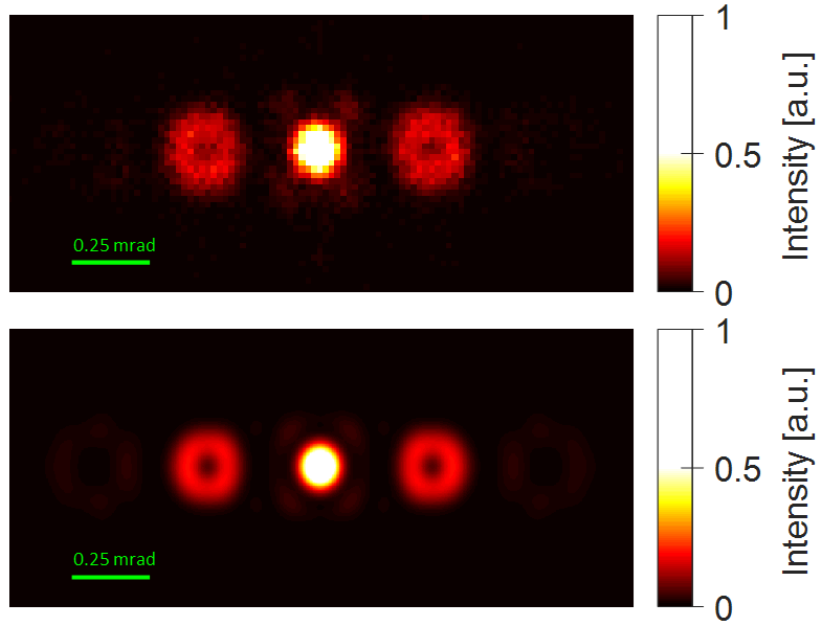
Figure S3: Calculated diffraction image for a circular aperture with a regular slit grating. The Airy disk image of a single aperture, which is a spot surrounded by concentric rings, become a series of spots with a surrounding structure. The spots do not contain the hole characteristic of the OAM beams due to the lack of the phase singularity. The images were calculated for a grating with an open to blocked slit ratio of 4/6.

<u>Neon vortex beam</u>

Our method for generating vortex beams of atoms and molecules can be applied to many species, owing to the generality of supersonic beam sources. As an example, we used our current setup to create vortices of neon atoms. We cooled the valve to 115K, producing a beam with a velocity of 550 m/s and a corresponding de-Broglie wavelength of 36 pm. Using $75~\mu m$ aperture skimmers, the coherence length was set to 680 nm. The DBD was applied to excite the atoms to metastable states, detectable with the MCP. The grating to detector distance was set to r_{GD}=215 cm to compensate for the smaller diffraction image of neon relative to helium.

Figure S4 presents images of diffracted neon atoms with the single-edge dislocation gratings used for the helium dimers. The first order rings are clearly visible on either side of the zero-order spot. The image also agrees very well with the simulated one obtained with the experimental parameters.

Figure S4: Diffraction images of neon atoms with a single-edge dislocation vortex grating. Top: Experimentally measured image, showing the $l = -1, 0, 1$ orders. (bottom) Simulated diffraction image. The intensity in both figures is saturated above 50% of the maximum value to emphasize the hole-structure appearing in the first order OAM rings.

Dimer identification

       The diffraction patterns with helium beams reveal additional spots centered at half the diffraction angles expected for atoms ("half-orders"). We attribute these spots to metastable helium dimers (He_2^*) produced by the DBD. These particles have a de-Broglie wavelength half that of the atoms. Such dimers are routinely created by discharges in supersonic valves at similar source conditions[39], especially at low temperatures and high pressures. We verify that these "half-orders" are likely dimers through two independent tests.

       First, the fraction of dimers formed during supersonic expansion of beams is strongly dependent of the beam parameters, as the collision rate (affected by local density and temperature) and total duration of the expansion influences the chance of association between atoms. With all other conditions constant, a lower valve temperature produces more dimers. We varied the temperature of the valve and measured the diffraction image to verify if the relative signal of the half-orders indeed changes as expected. Figure S5 presents a sample image for a valve temperature of 130 K; the squares indicate the division of the image into areas where detected events were allocated to the various orders. The center of each square matches the approximate center of the observed spots/rings. Table S1 presents the fraction of the total counts in these sections, for this temperature as well as for 100 K and 210 K. As would be expected for dimers, the fraction of particles in the half-orders falls significantly for higher temperatures.

       The second verification that these orders belonged to dimers was their lack of response to a laser locked to the 2^3S-2^3P atomic transition wavelength of 1083 nm. This test is depicted in Fig. S6, using a diffraction grating made of straight slits with a 100 nm periodicity, which exhibits both the atomic orders and these "half-orders". When we turn on the laser, the particles of atomic helium are deflected by many absorption events and heated due to the random emission directions. On the other hand, the "half-orders" remain unaffected. Note that this wavelength does not affect metastable atomic helium in the 2^1S state, thus these particles overlap with the even orders of the dimers.
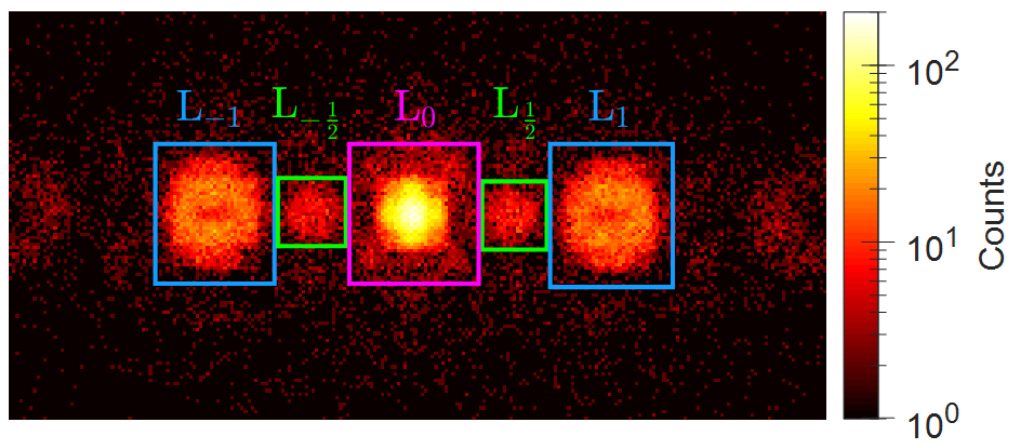
Figure S5: Division of the diffraction image into sections to test the effect of source temperature on the intensity of the "half-orders".

Valve temperature	Percent of events, out of total events in sections		
	L_0	$L_{-1} + L_1$	$L_{-1/2} + L_{1/2}$
100 K	48.2%	44.7%	7.1%
130 K	48.8%	45.5%	5.7%
210 K	50.2%	47.6%	2.2%

Table S1: The count rate of particles falling into sections allocated for "half-orders" decreases significantly with increasing temperature. This result matches the expected trend for metastable dimers formed in the expansion region.
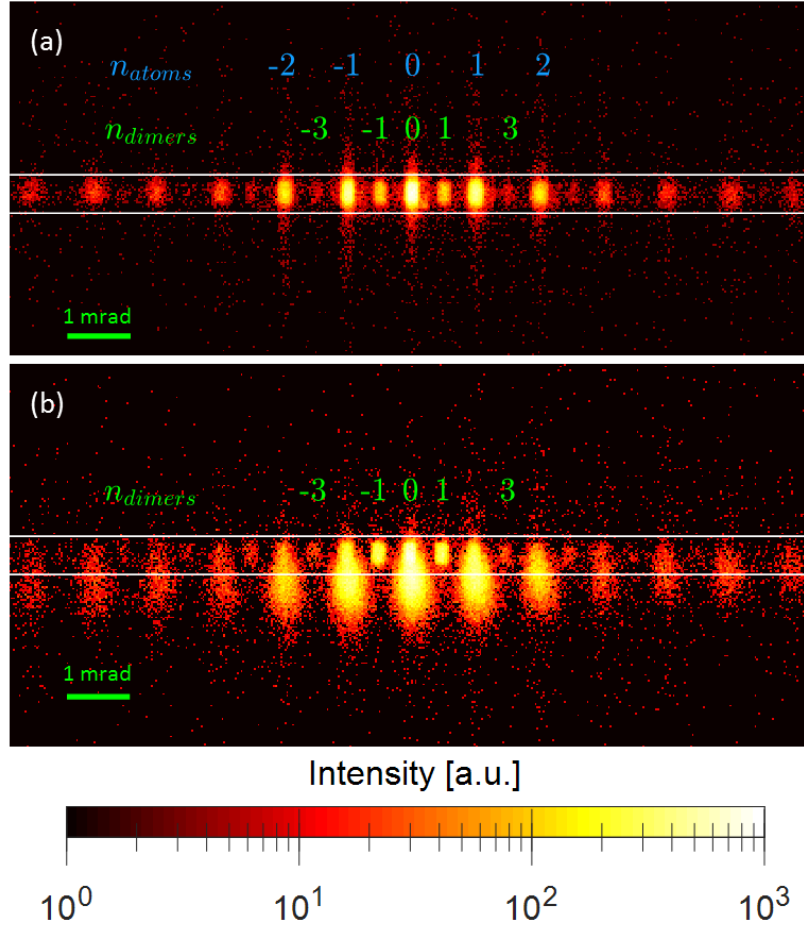
Figure S6: Diffraction images of helium beams impacting a regular transmission grating with a slit periodicity of 100 nm. The main diffraction orders are labeled by n and are associated to either atoms or dimers. The atomic beam in (a) freely propagates between the grating and the detector. In (b), a 1083 nm laser, resonant with the 2^3S-2^3P atomic transition coming from the direction above the detector, intersects the beam after the grating and deflects the triplet-state metastable atoms by photon scattering. The distorted orders belonging to these atoms show broadening due to heating, and the unaffected orders are associated with the helium dimers.